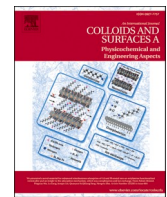




Contents lists available at ScienceDirect

Colloids and Surfaces A: Physicochemical and Engineering Aspects

journal homepage: www.elsevier.com/locate/colsurfa



Asphaltenes at the water-oil interface using DPD/COSMO-SAC

Fellipe C. de Oliveira ^a, João M. Maia ^b, Frederico W. Tavares ^{a,*}

^a Instituto Alberto Luiz Coimbra de Pós-Graduação e Pesquisa de Engenharia, Federal University of Rio de Janeiro, Av. Athos da Silveira Ramos, 149 - Bloco A, 2 andar - Cidade Universitária da Universidade Federal do Rio de Janeiro, Rio de Janeiro, Brazil

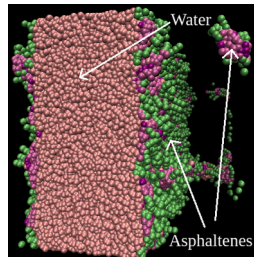
^b Department of Macromolecular Science and Engineering, Case Western Reserve University, Kent Hale Smith Building, 2100 Adelbert Rd, Cleveland, OH, United States



HIGHLIGHTS

- Mesoscale molecular simulation of asphaltenes at the water-oil interface.
- Asphaltene at the water-oil interface change orientation depends on concentration.
- COSMO-SAC method used to calculate the DPD parameters.
- Water-in-oil microemulsion stabilized by asphaltenes.

GRAPHICAL ABSTRACT



ARTICLE INFO

Keywords:

Asphaltene aggregation
Dissipative particle dynamics
COSMO-SAC
Molecular dynamics
Water/Oil interface

ABSTRACT

Asphaltenes are the heaviest fraction of crude oil. Its deposition causes large problems during oil exploitation. Sometimes it is difficult to separate the asphaltenes from the oil because of the very stable water in oil emulsions that they form. The Dissipative Particle Dynamics (DPD) has been used to study the interfacial properties of asphaltene molecules at the water-oil interface. The COSMO-SAC method was used to systematically obtaining the conservative force DPD parameters. The methodology to obtain the DPD-parameters has been tested in hydrocarbon-water systems yielding good results for the interfacial tension compared to experimental data. Asphaltene-toluene mixtures were also analyzed using this methodology in terms of diffusion coefficients and structural information showing consistent results. Ultimately, the water-asphaltene-oil systems were investigated, and the critical micelle concentration is in agreement with experimental values. Density profiles and angular analysis of asphaltene molecules at the water-oil interface have also been carried out, showing that those molecules are preferentially parallel to the interface at low asphaltene concentration, whereas at higher concentrations, entropic effects become dominant, and the molecules assume a tilted configuration. The size and number of aggregates at the water-oil interface show that asphaltenes form small aggregates at low concentrations and large structures at high concentrations.

1. Introduction

Asphaltenes are the heaviest fraction of the crude oil, and they are defined concerning their solubility characteristics. Asphaltene is the

component class that is soluble in aromatic solvents such as benzene, toluene and insoluble in n-alkane solvents such as hexane or pentane [1]. Asphalt is composed of many aromatic rings condensed at the molecule center surrounded by alkyl side chains [2]. Heteroatoms such

* Corresponding author.

E-mail address: tavares@eq.ufrj.br (F.W. Tavares).

as nitrogen, oxygen, and sulfur are also found in the central rings. Some metallic compounds such as nickel and vanadium can also be part of their structure [3]. The average molecular weight of those molecules is about 750 g/mol, with 4–10 aromatic rings and side chains composed of 3–7 carbons [4]. The asphaltene tendency to form aggregates in crude oil has been the object of study of many researches [5–7] as it can cause huge losses for the oil industry. Asphaltene aggregation influences the rheology, wettability, stability of water-oil emulsions and can agglomerates in pipelines causing flow assurance problems, which raises concerns around those molecules [8].

Removing water from the oil can be challenging in many cases because of the very stable water-oil emulsions which naturally emerge from the asphaltene molecules forming a film at the water-oil interface, which acts as an active surface molecule [9]. Experimentally, Bouriat et al. [10] observed that the asphaltene film formation at the interface between water and cyclohexane produces a cross-linked structure that ages with time. A clear sol-gel transition zone has been detected. The average adsorbed area was 2 nm^2 which indicates that isolated (or small clusters) molecules connect to the interface rather than large clusters. Chang et al. [11] measured the mechanical properties of the water-asphaltene-oil interface. They observed that asphaltenes increased the stiffness of the interface, causing a crossover from viscous to elastic dominated behavior. Heterogeneities at the interface have also been found, which led to anisotropic strain decay. Shi et al. [12] used atomic force microscopy (AFM) to measure the interfacial forces between water-oil emulsions droplets in organic solvent with adsorbed asphaltene molecules and found that the steric repulsion between asphaltene aliphatic chains inhibits coalescence, which caused droplet stabilization. The authors studied the asphaltene concentration influence in the adhesion forces between droplets. By using lateral shear, they were able to break up the asphaltene films, permitting droplets to coalesce.

Computationally, Molecular dynamics have also been carried out in an attempt to better understand the effects of asphaltene molecules at the water-oil interface. Liu et al. [13] studied the orientation of asphaltene molecules at the water interface by Molecular Dynamics (MD). The asphaltene molecules showed parallel stacking led by $\pi-\pi$ interactions between aromatic cores; the same molecules oriented perpendicular to the water interface. They also verified the demulsification by ethylcellulose, i.e., asphaltene molecules detaching from the droplets.

For large systems, mesoscale approaches are a promising tool [14, 15]. Those coarse-graining methodologies [16, 17] allow simulating large time and length scales by joining several atoms into a single particle. Dissipative Particle Dynamics (DPD) is a widespread coarse-graining method that has been used in many applications such as block copolymers [18], vesicle formation [19], the momentum transfer mechanisms mediated by Janus rods at polymer interfaces [20], surfactants [21], and carbon nanotubes [22]. Rezaei et al. [23] used DPD to study the behavior of asphaltene-like molecules with different terminal groups at the oil-water interface. They considered SARA crude oil model from the Persian Gulf as the oil composition and concluded that as the terminal groups became more polar, lower values of the interfacial tension (IFT) were obtained due to more significant interactions between side chains and water, which facilitates the water-oil separation. Ruiz-Morales and Mullins [24] constructed an asphaltene molecule model based on the DPD approach and tested different force field parameters. They found that the molecular planes stay parallel to the water-oil interface while the alkyl chains are perpendicular. Some asphaltene molecules went to the oil phase due to steric repulsion and jamming. Silva [25] using experimental solubility parameters, calculated the Flory-Huggins interaction parameters and then the DPD conservative parameters based on the Groot and Warren [16] methodology. The IFT evolution of the asphaltene-oil interface as a function of the polarity degree of different solvents was performed. In pentane, the highest IFT (interface emergence) was observed, while in benzene the lowest IFT (dissolution) was obtained, that agrees with

experimental results. Wang et al. [26] used GPU-accelerated DPD simulations to study heavy, light, and emulsion crude oil systems. The asphaltenes formed large aggregates in their heavy crude oil, which enhances the suspension viscosity. The addition of light fractions lowered the asphaltene mass fraction and aggregate size, which also increased the Newtonian suspension behavior. Regarding the asphaltene surfactant characteristics, they observed that asphaltene molecules increased the dispersion of the emulsions. Chen et al. [27] studied the structure and orientation of asphaltene molecules at the oil-water interface using both continental and archipelago-like structures by means of DPD and found that the change from parallel to perpendicular molecular orientation occurs when archipelago-like molecules replace continental molecules. They also observed that the presence of heteroatoms in the asphaltene molecules is the main drive force leading to the molecule adsorption at the interface, while the aromatic cores are responsible for parallel molecular stacking. de Oliveira et al. [28] studied the viscoelastic behavior of asphaltene model molecules using the DPD coarse-graining method in toluene and heptane. They were able to describe the structural and dynamical properties of those molecules according to the solvent used. The authors also tested several mass fractions and concluded that the increase of the mass fraction causes an increase in the viscosity, which is higher in toluene because its viscosity is higher than the heptane viscosity. In the same work, oscillatory rheology was promoted by molecular simulations, and the results showed that at the initial aggregation stages, the suspensions have higher liquid-like behavior, which is confirmed by experimental results.

COSMO methodologies have been used for calculating many substance properties. Fingerhut et al. [29] tested two COSMO-SAC models: COSMO-SAC2010 [30] model and COSMO-SAC-dsp [31]. COSMO-SAC2010 [30] model improvement over the original COSMO-SAC [32], lies in the recognizing different strengths of hydrogen bonding interactions, which depends on the type of hydrogen bonding donors and acceptors. Whereas COSMO-SAC-dsp has a correction term based on molecular simulation data, taking into account the dispersive intermolecular interactions explicitly. The authors have proven that the latter presents a lower mean absolute deviation of the infinity dilution activity coefficient, being more accurate. Merker et al. [33] analyzed the gas solubility of oxygen, CO_2 and their mixtures. They compared experimental data, molecular simulation, and COSMO-SAC. COSMO-SAC results were far better than the Peng-Robinson equation of state as in predictive as in adjusted mode. Lee and Lin [34] developed a new method to screen ionic liquids to be used in the CO_2 capture process. They used COSMO-SAC to calculate de infinity dilution activity coefficient of the gas in the ionic liquid. The substances CO_2 , CH_4 , N_2 and H_2 were tested in terms of solubility, selectivity, and the temperature dependency of solubility, showing promising results. Their methodology is promising in screening the best ionic liquid candidates for CO_2 capture. Soares [35] and Gerber and Soares [36] developed and provided new and free software to determine activity coefficients from COSMO-SAC named JCOSMO. They recalibrated the COSMO-SAC model and compared infinity dilution activity coefficient with UNIFAC (Do) [37–39]. Their COSMO-SAC implementation showed better agreement with experimental data for molecules with several functional groups or when functional groups appear in an unusual way, which reinforces this new methodology as a promising tool. Alasiri and Chapman [40] used COSMO-RS to calculate the DPD interaction parameters studying the alkane-water interface and demonstrated that their methodology is capable of reproducing quite well the IFTs of those systems. Dmol3 commercial software was used to obtain the infinity diluted activity coefficient required. Alasiri et al. [41] used the same method to study the effect of head groups, salts, and temperature on interfacial properties of water-octane-surfactant systems. They used sodium dodecyl sulfate (SDS), dodecyltrimethylammonium bromide (DTAB), and dodecyldimethylamine oxide (DDAO) as surfactants. Experimental

IFTs were obtained from pendant drop method, which agreed semi-quantitatively with DPD simulations.

A molecular dynamics study of the asphaltene surfactant properties at the water/oil interface is still in lack in the literature. Here, the COSMO-SAC method was used to evaluate the DPD-binary-interaction parameters between asphaltene, water, and cyclohexane beads. To verify the quality of these parameters and the ability of the DPD in describing the thermodynamic properties, we calculated the interface tension (IFT) of different hydrocarbons and water and compared those with experimental data. The asphaltene structural properties and diffusion coefficient were also calculated to verify if this new methodology can reproduce experimental data of diluted asphaltene in toluene. The first peak of the radial distribution function ($g(r)$) occurs about 5.08 Å, and the diffusion coefficient of diluted asphaltene in toluene (5% and 10% mass fractions) agrees well with experimental literature data. Simulations of asphaltene at the water-oil (cyclohexane) interface were run, and the obtained IFTs agree well with the experimental available data in terms of CMC (critical micelle concentration). This is the first time that a mesoscale molecular dynamics study has been able to capture the asphaltene surfactant characteristics. This new methodology based on free COSMO-SAC software has proven to be very simple and useful in determining the characteristics of asphaltene molecules acting as surfactant at the water-oil interface.

2. Methodology

2.1. The computational method

Hoogerbrugge and Koelman [42] have proposed the DPD method as a simulation algorithm designed for mesoscale simulations that include hydrodynamic effects. It combines molecular dynamics [43] features with lattice gas automata [44], being faster than the former and more flexible than the latter. Thenceforth the DPD method has been used for simulating the behavior of complex fluids. In this method, each particle corresponds to a collection of real atoms/molecules, enabling the simulation of ample time and length scales. In DPD, the total force acting on a particle i (\mathbf{F}_i) is composed of three forces: conservative ($\mathbf{F}_{ij}^C(\mathbf{r}_{ij})$), dissipative ($\mathbf{F}_{ij}^D(\mathbf{r}_{ij}, \mathbf{v}_{ij})$), and random ($\mathbf{F}_{ij}^R(\mathbf{r}_{ij})$). The expression forces are as follows:

$$\mathbf{F}_i = \sum_{j \neq i} (\mathbf{F}_{ij}^C(\mathbf{r}_{ij}) + \mathbf{F}_{ij}^D(\mathbf{r}_{ij}, \mathbf{v}_{ij}) + \mathbf{F}_{ij}^R(\mathbf{r}_{ij})) \quad (1)$$

$$\mathbf{F}_{ij}^C = -a_{ij}\omega^C(r_{ij})\hat{\mathbf{r}}_{ij} \quad (2)$$

$$\mathbf{F}_{ij}^D = -\gamma\omega^D(r_{ij})\hat{\mathbf{r}}_{ij}(\mathbf{v}_{ij} \cdot \hat{\mathbf{r}}_{ij}) \quad (3)$$

$$\mathbf{F}_{ij}^R = \sigma\omega^R(r_{ij})\hat{\mathbf{r}}_{ij}\zeta_{ij}/\sqrt{\delta t} \quad (4)$$

Where \mathbf{r}_{ij} and \mathbf{v}_{ij} are the distance and relative velocity vectors, therefore $\mathbf{r}_{ij} = \mathbf{r}_j - \mathbf{r}_i$ and $\mathbf{v}_{ij} = \mathbf{v}_j - \mathbf{v}_i$. \mathbf{r}_i and \mathbf{v}_i are governed by the Newton equations of motion: $\frac{d\mathbf{r}_i}{dt} = \mathbf{v}_i$, $m_i \frac{d\mathbf{v}_i}{dt} = \mathbf{F}_i$, wherein m_i is the mass of bead i . $\hat{\mathbf{r}}_{ij}$ is the unit vector in \mathbf{r}_{ij} direction, r_{ij} is the modulus of \mathbf{r}_{ij} . All forces act until the cutoff distance r_c . ζ_{ij} is a random number with zero mean and unit variance that follows a Gaussian distribution. $\omega^C(r_{ij})$, $\omega^D(r_{ij})$, and $\omega^R(r_{ij})$ are the weight functions related to the respective forces. a_{ij} , γ and σ are the parameters of conservative, dissipative, and random forces, respectively.

The conservative force represents the chemical nature of the DPD particles and should reproduce the thermodynamics (in terms of compressibility) of the system. The dissipative force models the friction between particles related to the viscosity at the mesoscale (hydrodynamics). The random force mimics the Brownian motion, which gives energy to the system. Espanol and Warren [45] showed that the random and dissipative forces must satisfy the fluctuation-dissipation theorem [46] to maintain the temperature of the system constant. Resolving the

fluctuation-dissipation theorem for DPD, they found the following requirements to simulate the NVT canonical ensemble [47]:

$$\omega^C(r_{ij}) = 1 - \frac{|\mathbf{r}_{ij}|}{r_c} \quad (5)$$

$$\omega^D(r_{ij}) = [\omega^R(r_{ij})]^2 = \left(1 - \frac{|\mathbf{r}_{ij}|}{r_c}\right)^2 \quad (6)$$

$$\gamma = \frac{\sigma}{2k_B T} \quad (7)$$

Other potentials were also included to simulate the asphaltene structure:

$$E_{bond} = K_{bond}(r - r_0)^2 \quad (8)$$

$$E_{angle} = K_{angle}(1 - \cos(\theta - \theta_0)) \quad (9)$$

$$E_{improper} = K_{improper}(1 + d\cos(n\phi)) \quad (10)$$

Where E_{bond} , E_{angle} , and $E_{improper}$ are the bond, angle and improper potentials [48]. The K_{bond} , K_{angle} , and $K_{improper}$ are the constants for those potentials which were determined to maintain the asphaltene molecule flat without increasing the system temperature. Descriptions of these forces are found in LAMMPS package [48] documentation.

3. Coarse-graining and simulation details

The simulations performed in this work were carried out using the LAMMPS package [48], which has been chosen because of parallelization. The dissipative and random force parameters used were $\gamma = 4.5$ and $\sigma = 3$ in DPD units as determined by Groot and Warren. For the DPD method each bead corresponds to N_m (degree of coarse-graining) water molecules. Following the coarse-graining of Alasiri et al. [41], $N_m = 4$ (see Fig. 1), which means that each DPD bead corresponds to the volume of 4 water molecules for the coarse-graining used here. The total system numerical density ρ was set to 3 (in DPD units) [16]. According to Groot and Rabone [49] the length (r_c), mass (m) and time (τ) scales are calculated by:

$$r_c = (\rho N_m V_W)^{1/3} \text{ Å} \quad (11)$$

$$m = N_m m_{water} \text{ amu} \quad (12)$$

$$\tau = r_c \sqrt{m/(k_B T)} \text{ ps} \quad (13)$$

Where m_{water} is the mass of one water molecule, and V_W is the molecular volume of one water molecule. The volume of one water molecule is about 25.74 Å [50]. Therefore, for this coarse-graining the volume of one water bead is 102.96 Å. The length, mass, and time scales used here are then $r_c = 6.76$ Å, $m = 72$ amu, and $\tau = 3.64$ ps. The equilibrium temperature was set at 298 K, which means that the energy scale $k_B T$ in physical units is 0.59 kcal/mol. A timestep of 7.29 fs (0.002τ) was used in a cubic box and periodic boundary conditions were applied in each direction.

Determining coarse-graining models for real molecules is not a simple task, many authors [8,27,51–54] have proposed DPD methodologies and were able to reproduce the structural/dynamical characteristics of asphaltene suspensions. Espanol and Warren [55] published a article reviewing the main DPD coarse-graining approaches and commenting about their advantages/disadvantages. The asphaltene molecule used here was obtained from Song et al. [51], Fig. 1. Even though asphaltene molecular structure is not completely understood [56], it is known that its hypothetical configuration is constituted of aromatic rings, alkyl side chains and heteroatoms. Fig. 1 shows the molecular structure that was used here; it has a island structure, which means that it is formed by many central rings surrounded by side chains. This structure is referenced as “like hand” structure, with the palm represented by the central core and

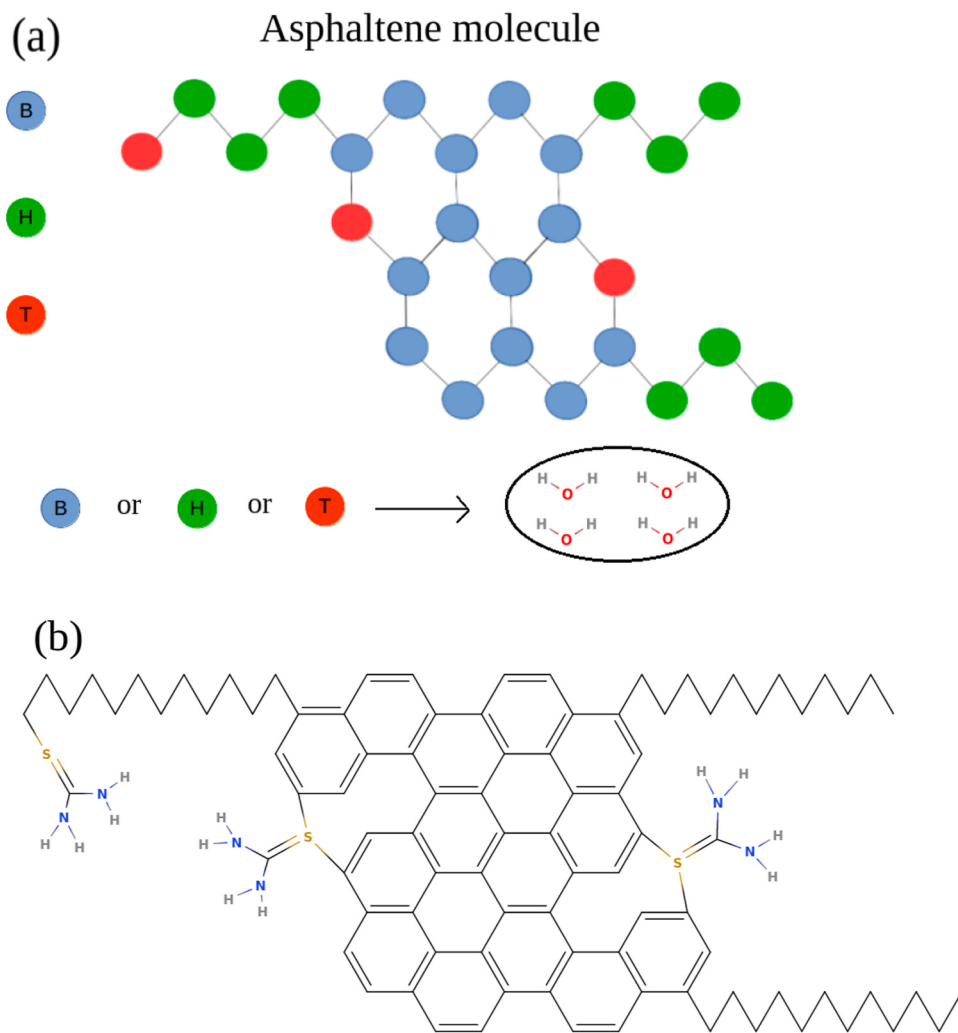


Fig. 1. (a) Asphaltene molecular structure representation: B bead (blue) represents a moiety of aromatic rings which is the benzene in this approach, H bead (green) represents a butane molecule which forms the alkyl side chains, T bead (red) represents the thioglycolic acid molecule which is the heteroatom group. Each bead corresponds to the volume of 4 water molecules. (b) The structural formula of the hypothetical asphaltene molecule model used in this work. The heteroatoms were described in detail. (For interpretation of the references to color in this figure legend, the reader is referred to the web version of this article.)

fingers representing side chains. Three types of particles were used: B bead (blue) represents a moiety of aromatic rings which represents the benzene, H bead (green) represents a butane molecule which forms the alkyl side chains, and T bead (red) that represents the thioglycolic acid molecule which has been chosen as the heteroatom group, having greater affinity to water than the other beads.

In the DPD method, all particles should have approximately the same size [57]. Water, n-butane, benzene, thioglycolic acid, toluene, n-propane, n-decane, and cyclohexane have been used, the molecular volumes were obtained from Mullins et al. [50]. Table 1 shows that all beads have almost the same size considering the coarse-graining of each molecule, as required by DPD method. The bond constant force K_{bond} , Eq. (8), was set to 1000 for bonds between beads in the polycyclic asphaltene nuclei, and 100 for the alkyl side chain bonds, while the

equilibrium distances r_0 were 0.8 and 0.9, respectively. The angle constant K_{angle} , Eq. (9), was 125, and the equilibrium angle $\theta_0 = 120^\circ$. For the improper expression energy, Eq. (10), the parameters were set as $K_{improper} = 5$, $d = -1$ and $n = 2$ to keep the asphaltene molecule flat. All in DPD units. The improper potential acts between quadruplets of beads [58]. According to the asphaltene molecule used here, see Fig. 1, it acts between beads BBHT, BBBB, BBBH, and BBBT.

Groot and Warren running a series of simulations varying the numerical density ρ and values of the like-like bead conservative interaction a_{ii} , have found the following relationship between a_{ii} and ρ , $a_{ii}\rho = 75k_BT$. Thus, the interaction parameter between equal beads is 25, in DPD units, for $\rho = 3$. The same authors, aiming to find a method to determine the unlike-unlike (a_{ij}) bead conservative interaction, used the Flory-Huggins polymer solution theory to establish a linear expression between a_{ij} and the Flory-Huggins interaction parameter χ_{ij} :

$$\chi_{ij} = 0.286(a_{ij} - a_{ii}) \quad \text{for } \rho = 3 \quad (14)$$

Table 1
Bead sizes of molecules studied in this work, data taken from Mullins et al. [50].

| Molecule | Size (\AA^3) |
|-------------------|-------------------------|
| n-Butane | 102.43 |
| Benzene | 110.22 |
| Cyclohexane | 129.72 |
| n-Decane | 233.48 |
| n-Propane | 80.70 |
| Thioglycolic acid | 102.99 |
| Toluene | 132.25 |
| Water | 25.74 |

A methodology for the calculation of the Flory-Huggins parameter is necessary to determine the unlike bead interaction a_{ij} . In this approach, the Flory-Huggins lattice theory is used to match the phase behavior of real fluids and the DPD method. The COSMO-SAC (conductor-like screening segment activity coefficient) theory [32] has been created by Lin and Sandler as a strategy to obtain the thermodynamic properties of liquids and liquid mixtures. It is based on COSMO [59], which uses quantum calculations to calculate the dielectric screening energy in solvents. Cosmo-based methods move a molecule from vacuum to a perfect

conductor and then to a real solvent medium. More details about the COSMO-based procedure can be found elsewhere [32,59–62]. Alasiri and Chapman [40] have found a relationship between the infinity dilution activity coefficient (γ) and the Flory-Huggins parameter χ for a solute (i)/solvent(j) system:

$$\chi_{ij}^{\infty} = \ln(\gamma_i)^{\infty} + \ln(\nu_{ij}) - (1 - \frac{1}{\nu_{ij}}) \quad (15)$$

Where γ_i^{∞} is the infinity dilution activity coefficient, and ν_{ij} is the volume ratio between the solute and solvent. The estimation of the activity coefficient is made by COSMO-SAC, using the free software JCOSMO [35,36], which was developed by Soares [35] and Gerber and Soares [36]. It is clear that having the tools for calculating the activity coefficient between two components, using Eq. (15) and then Eq. (14), it is possible to calculate the unlike conservative interaction between two different beads.

4. Results and discussion

4.1. Hydrocarbon-water systems

Firstly, Dissipative Particle Dynamics was used to simulate the interfacial characteristics of alkane-water systems. A box of $23 r_C \times 23 r_C \times 31.5 r_C$ with $5 \cdot 10^4$ beads has been created, half of the beads being water and half composing the alkanes. Periodic boundary conditions were applied, and in the initial condition, all particles were placed randomly within the simulation box. A total of $6 \cdot 10^5$ timesteps were carried out ($\Delta t = 0.002\tau$), among which the first 20% were equilibration steps, followed by the production steps. The interfacial properties of hexane, octane, and dodecane were tested in water. To keep a consistent coarse-graining degree, the hexane molecule was created with 2 propane beads ($N_m = 3$), while octane and dodecane were composed of 2, and 3 butane beads, respectively, maintaining $N_m = 4$. The alkanes are treated as bonded monomers of propane and butane. The IFTs were calculated by [63]:

$$\text{IFT} = \frac{1}{2} \left(P_{zz} - \frac{P_{xx} + P_{yy}}{2} \right) L_z \quad (16)$$

Where P_{xx} , P_{yy} , and P_{zz} are the diagonal components of the system stress tensor for the equilibrated system. L_z is the z box edge length. To convert this DPD unit value into real units, we used a factor of $k_B T / r_C^2$. Initially, all particles are randomly dispersed in the simulation box. After the equilibrium has been reached, the system separates into two phases, forming two well-defined interfaces (due to the periodic box). The 1/2 factor multiplying Eq. (16) is due to those two interfaces that are formed, as shown in Fig. 2.

The interaction parameters between water and hydrocarbon beads were calculated by using Eqs. (15), (14). The Flory-Huggins parameters (χ_{ij}^{∞}) were calculated using the infinity dilution activity coefficients from JCOSMO for different temperatures. According to Maiti and McGrother [57], the a_{ij} parameters should be scaled, taking into account the bead size. In Eq. (15), there are discrepancies between the water and alkane molecular volume because one water bead is supposed to include N_m water molecules. Hence, avoiding these unphysical size discrepancies requires multiplying χ_{ij}^{∞} by N_m before calculating a_{ij} . That scaling does not affect the a_{ii} value. So that:

$$\chi_{ij}^{\infty}(N_m) = N_m \chi_{ij}^{\infty} \quad (17)$$

As the Flory-Huggins parameters are temperature dependent, we could find a linear relationship between the a_{ij} parameters and the temperature. For the bead interactions promoted in this section, the results are shown in Table 2. As the bead size increases, the a_{ij} also increases, meaning that the repulsion between water and larger alkanes is higher than with small alkanes. The slope of the fits are negative, which means that as the temperature increases, a_{ij} decreases, resulting in better affinity between water/

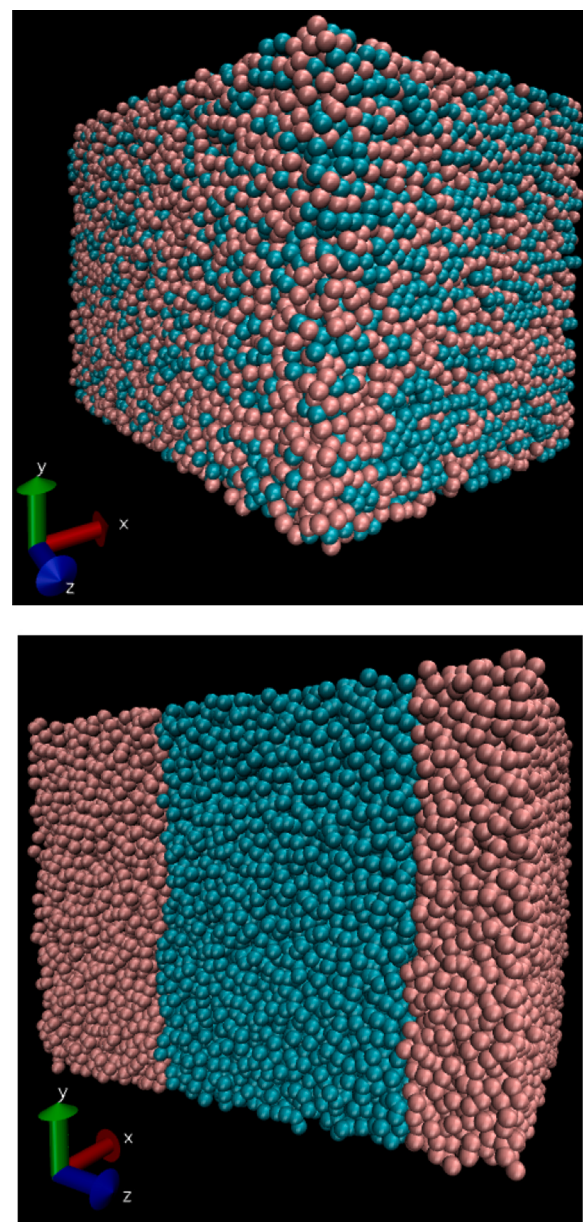


Fig. 2. Water-octane molecular simulation at the initial step and at the final equilibration step. Water is represented by blue beads, whereas octane by pink beads. Two interfaces naturally form, which leads to a 1/2 multiplication prefactor in Eq. (16). (For interpretation of the references to color in this figure legend, the reader is referred to the web version of this article.)

Table 2

Linear relationship between water and hydrocarbon bead interaction parameters a_{ij} and the temperature. χ_{ij}^{∞} were calculated before scaling, Eq. (15). $\chi_{ij}^{\infty}(N_m)$ calculated after scaling, Eq. (17). a_{ij} calculated using $\chi_{ij}^{\infty}(N_m)$ values in Eq. (14).

| Bead | χ_{ij}^{∞} | $\chi_{ij}^{\infty}(N_m)$ | a_{ij} | R^2 |
|-------------|--------------------------|---------------------------|---------------------------|-------|
| n-Butane | -0.013 · T°C + 8.988 | -0.050 · T°C + 35.954 | -0.176 · T°C + 150.712 | 0.999 |
| Propane | -0.010 · T°C + 7.582 | -0.031 · T°C + 22.745 | -0.108 · T°C + 104.528 | 0.999 |
| Benzene | -0.006 · T°C + 6.726 | -0.025 · T°C + 26.903 | -0.088 · T°C + 119.067 | 0.999 |
| Cyclohexane | -0.015 · T°C + 10.396 | -0.059 · T°C + 41.584 | -0.205 · T°C + 170.397 | 0.999 |
| n-Pentane | -0.014 · T°C + 10.350 | -0.074 · T°C + 51.750 | -0.257 · T°C + 205.941 | 0.999 |

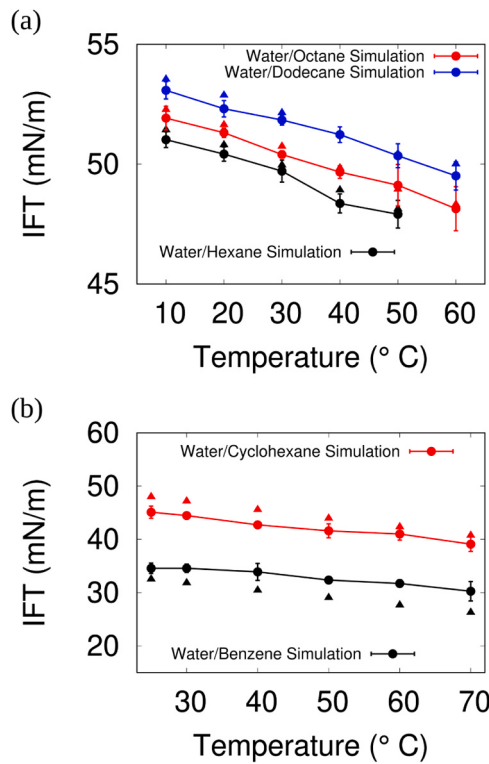


Fig. 3. (a) Water/alkane IFT calculation for different temperatures using DPD. The circular points are the DPD simulations, while the triangle points are the experimental data [64]. (b) Water/benzene and water/cyclohexane IFT calculation for different temperatures using DPD. The circular points are DPD simulations, while the triangle points are the experimental data [65]. Black points represent water/benzene data; red points represent water/cyclohexane data. Standard deviations are shown as error bars. Experimental error bars are too narrow, seeming not visible. (For interpretation of the references to color in this figure legend, the reader is referred to the web version of this article.)

alkanes at higher temperatures. The slope decay is almost the same for the two interaction types. Even though the classical Flory-Huggins parameter in DPD [16] depends on the interaction energy between species, numerical densities, and temperature, it is also dependent on the two species sizes in this strategy.

Simulations were conducted varying the temperature to compare our results with Zeppieri et al. [64]'s experimental data. Fig. 3(a) shows the IFT curve against temperature for the water/alkane systems. The triangle points are the experimental values, while the circular points are the DPD simulated values. The error bars denote the standard deviations. The experimental error bars are too narrow, seeming not visible. In all cases, the match between the experimental and simulated data falls within the standard deviation and even when that is not the case, the differences are relatively small quantitatively. Therefore, it is valid to consider that the simulations can adequately capture the IFT of these systems.

Table 3

Diffusion coefficient D for asphaltene solutions in toluene for different mass fractions $X = 0.02, 0.05, 0.10$, and 0.15 . D values are higher for low concentrations as a consequence of higher mobility. Low concentration D values are within the experimental range $2.2\text{--}6.3 \cdot 10^{-10} \text{ m}^2/\text{s}$ [68,69].

| Mass fraction | Diffusion coefficient D (m^2/s) |
|---------------|---|
| 0.02 | $5.2 \cdot 10^{-10}$ |
| 0.05 | $2.9 \cdot 10^{-10}$ |
| 0.10 | $8.2 \cdot 10^{-11}$ |
| 0.15 | $5.3 \cdot 10^{-11}$ |

The same strategy was applied to calculate the interfacial tension of cyclohexane and benzene in water. The simulated conditions were the same. The DPD parameters are shown in Table 2, while the IFT curves compared to experimental values are presented in 3(b). The IFT results for benzene and cyclohexane in water were not as close to experimental data as the previous ones. It seems that the larger the degree of coarse-graining is, or more polar the molecule, the less accurate the model is, which will be the object of further studies.

4.2. Asphaltene solutions in toluene

Here, we investigated the ability of the proposed strategy to reproduce the characteristics of asphaltene in toluene solutions. Toluene was chosen as the solvent due to the experimental data related to it regarding asphaltene suspensions. For these simulations, a box of $27.14 r_C \times 27.14 r_C \times 27.14 r_C$ with $6 \cdot 10^4$ beads has been created. The mass fractions $X = 0.02, 0.05, 0.10$, and 0.15 were tested. Periodic boundary conditions were applied, and initially, all particles were placed randomly within the simulation box. A total of $6 \cdot 10^6$ timesteps were carried out with $\Delta t = 0.002\tau$, among which the first 50% were equilibration steps, followed by the production steps. The coarse-graining degree for all beads is again $N_m = 4$. The asphaltene molecular structure and molecule parameters were described in the Section 3. The interaction parameters between beads were calculated at 298.15 K using the methodology described previously. Those parameters are exhibited in Table 4.

Firstly, the radial distribution function $g(r)$ of asphaltene molecules was calculated to obtain the interlayer distance between molecular centers d . The center-to-center $g(r)$ was calculated considering the distance between center of mass of asphaltene molecules. The radial distribution function is calculated by dividing the local density by the overall density of the system ρ_a , which in this case is the number of asphaltene molecules divided by the volume. The $g(r)$ first step calculation is performed counting the number of centroids N_r retained in a shell of volume ΔV at a distance r from a specified centroid. The local density is obtained dividing N_r by ΔV , which is ensemble-averaged and then divided by the bulk density ρ_a of the system:

$$g(r) = \langle \frac{N_r}{\Delta V} \rangle \frac{1}{\rho_a} \quad (18)$$

Where $\langle \rangle$ means ensemble average. The Coordination Number N_c determines the number of neighbors around a central atom, it is the integral of $g(r)$:

$$N_c(r) = \int_0^r \rho_a g(r') 4\pi r'^2 dr' \quad (19)$$

Fig. 4 shows the radial distribution function for all asphaltene concentrations against dimensionless distance. Fig. 5 shows the Coordination Number N_c curves. As $N_c \geq 1$ for all cases at the first minimum of $g(r)$, the systems are surely aggregated. The first peak of $g(r)$ represents the first shell of aggregation, which is related to the interlayer distance d . The interlayer distance obtained in this work is about 5 Å, other authors found similar results by molecular simulation [28,66]. This value is a little higher than the experimental distance 3–4 Å [54,6,67], which is explained by the fact that asphaltenes also aggregate with an

Table 4

The a_{ij} conservative repulsion parameters for the DPD force field between asphaltene, water, toluene, and cyclohexane beads. The parameters were calculated using Eqs. (15), (17), and (14). Infinity dilution activity coefficients were taken from JCOSMO [35,36] at 298.15 K. Results in DPD units.

| | Water | Cyclohexane | Benzene | Butane | Thioglycolic-acid | Toluene |
|-------------------|-------|-------------|---------|--------|-------------------|---------|
| Water | 25 | 165.36 | 116.86 | 146.15 | 7.19 | 134.39 |
| Cyclohexane | | 25 | 35.98 | 25.57 | 129.46 | 27.10 |
| Benzene | | | 25 | 33.93 | 76.08 | 25.40 |
| Butane | | | | 25 | 126.40 | 31.20 |
| Thioglycolic-acid | | | | | 25 | 81.28 |
| Toluene | | | | | | 25 |

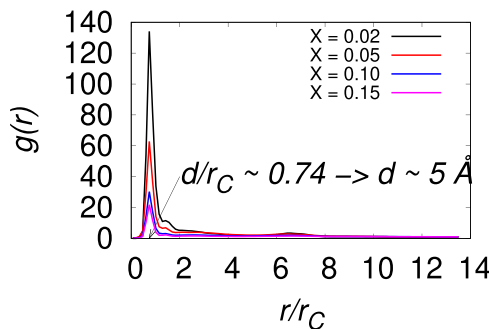


Fig. 4. Radial Distribution Function $g(r)$ for asphaltene in toluene solutions. The interlayer distance between molecular centers d is represented by the first peak distance, which represents the first shell of aggregation. It is seen that for all concentrations, the interlayer distance d is $\sim 5 \text{ \AA}$, which agrees with several molecular dynamics studies [28,66].

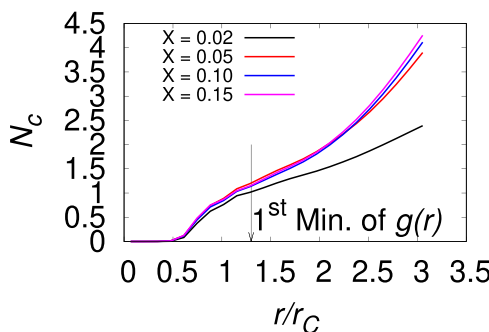


Fig. 5. Coordination Number N_c curves. As $N_c \geq 1$ for all cases at the first minimum of $g(r)$, the systems are surely aggregated.

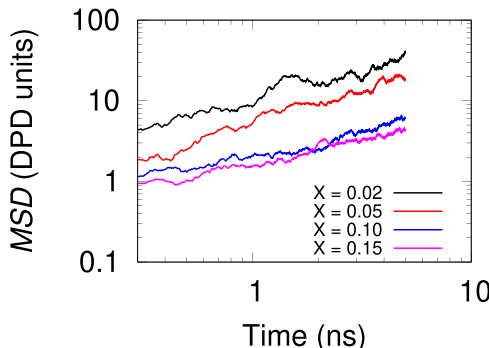


Fig. 6. MSD curves for asphaltene solutions in toluene at different mass fractions $X = 0.02, 0.05, 0.10$, and 0.15 . At higher concentrations, the MSD decreases because of lower particle mobility.

offset displacement between their molecular centers [4], increasing the distance between them.

The Mean Square Displacement (MSD) has also been computed for the center of mass of asphaltene molecules. It is calculated by:

$$MSD(t) = \frac{1}{N_{total}} \sum_{n=1}^{N_{total}} (r_n(t) - r_n(0))^2 \quad (20)$$

Where r_n is the position of a specified centroid n , and N_{total} is the total number of asphaltene molecules. The $(r_n(t) - r_n(0))^2$ is the squared displacement of a molecule center n at time t , then the MSD is a measure of the molecular mobility. Fig. 6 shows the MSD curves for the asphaltene solutions in toluene. As the mass fraction increases, the MSD values decrease as a consequence of the lower mobility caused by a higher concentration. The diffusion coefficient D is the derivative of the MSD with respect to time and for the three-dimensional case, it is given by Eq. (21). As the simulation proceeds, the asphaltene molecules aggregate, which arrests their movement [28], evidence of a sol-gel transition of asphaltene solutions [1,10] appears. If the system is completely arrested, at long times, very high concentrations and very low temperatures, the MSD tends to a constant value and the diffusion coefficient is zero. Therefore, to calculate diffusion coefficient, short and very long time-scales are neglected; it should be calculated in the MSD linear region, which is plotted in Fig. 6. Table 3 shows the calculated diffusion coefficients for the different concentrations, and it is noticeable that at low concentrations, the diffusion coefficient agrees well with the experimental data for the infinite dilution diffusion coefficient of asphaltenes in toluene $2.2\text{--}6.3 \cdot 10^{-10} \text{ m}^2/\text{s}$ [68,69].

$$D(t) = \frac{1}{6} \frac{d(MSD(t))}{dt} \quad (21)$$

4.3. Asphaltenes at the water-oil interface

As asphaltene molecules act as surfactants at the water-oil interface, the water-asphaltene-cyclohexane system was selected to study

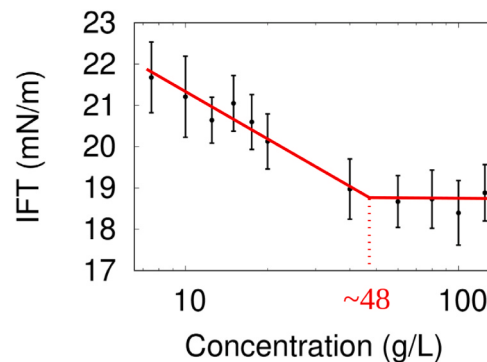


Fig. 7. Interfacial tension of asphaltenes at the water/cyclohexane interface at 298 K. Results from molecular simulation using DPD/COSMO-SAC. Standard deviations represented by error bars. Red lines to guide the eyes. The CMC is about 48 g/L. (For interpretation of the references to color in this figure legend, the reader is referred to the web version of this article.)

the interfacial properties of asphaltenes. For these simulations, concentrations in the range 7.5–150 g/L were carried out. Periodic boundary conditions were applied. The number of timesteps, and the value of the timestep is the same as in the previous section, the first 25% were equilibration steps, followed by the production steps. Again, the coarse-graining degree for all beads is $N_m = 4$, meaning that every bead is composed of 4 water molecules. The asphaltene molecular structure and molecule parameters were described in the Section 3. The interaction parameters between beads were calculated at 298.15 K, those parameters are exhibited in Table 4.

Experimental data for the interfacial tension of the water-asphaltene-cyclohexane systems at 298 K was published by Bouriat et al. [10]. The simulated interfacial tension of asphaltenes in water/cyclohexane is plotted in Fig. 7. Our goal is not to try to reproduce the experimental data, since it is not possible to determine the exact asphaltene molecular

structure. That being said, from experimental data, it can be seen that the IFT has a decreasing tendency until ~ 17.5 g/L [10], becoming constant afterwards. This constant value can be thought of as the CMC (critical micelle concentration) of the asphaltenes, i.e., this value represents the interface saturation. Loh et al. [70,71] reported CMC values for asphaltenes ranging from 1 to 30 g/L depending on the solvent used. The CMC found in this work is about 48 g/L, which is a good indicator of the reliability of the proposed modeling. Fig. 8 shows the initial micelle formation at about 48 g/L.

At concentration 125.0 g/L the interfaces are supersaturated and asphaltene molecules start forming a complex interface which is more evident at 150.0 g/L. At 150.0 g/L the interfaces are no longer planar which makes impossible to calculate the IFT by the methodology used here. The surface geometry becomes spherical-like resembling droplets, which indicates the formation of microemulsions. Figs. 9 and 10 show the interfaces formed at higher concentrations.

The Linear Density Profile (LDP) has also been calculated to study the interface structure. The LDP is calculated along one direction, see Giorgino [72] for further details. Fig. 11 shows an example of the LDP for asphaltene concentration 40.0 g/L, curves were normalized by their maximum value to be on the same scale. The asphaltene profile has two peaks representing the two interfaces formed, and both have almost the same peak value, which means that the system is well equilibrated with homogeneous interfaces (the same number of molecules at each interface). The water and oil profiles were also plotted, it is seen that the asphaltene profile is within the interfaces. A small lateral peak in the asphaltene profile represents the water in oil micelle formation.

The LDP values were integrated and then divided by 2 to calculate the number of molecules at the interface (NI). The plot is shown in Fig. 12 against asphaltene bulk concentration. It is seen that the higher the bulk concentration is, the higher the number of molecules per interface is. The asphaltene molecules that are inside the oil phase at higher concentrations were excluded in the integration of LDP. From Fig. 12, we notice two regimes, showing by lines (to guide the eyes). The interception is at approximately the same CMC concentration.

The angle θ between the asphaltene molecular planes and the interfaces has also been calculated, see Fig. 13. The asphaltene molecular plane is defined as the plane α . The molecular plane vector \vec{v} is defined as the position vector between the first and last particle position of the polycyclic aromatic nuclei, as indicated in Fig. 13. The vector \vec{n} normal to the xy plane (interface occurring in the z direction) is $(0,0,1)$. Therefore, the acute angle θ between the straight line \vec{v} and the plane defined by the normal \vec{n} is calculated by Eq. (22):

$$\sin\theta = \left| \frac{\vec{v} \cdot \vec{n}}{|\vec{v}| |\vec{n}|} \right| \quad (22)$$

Aiming at improving the sample of the angle profiles, we calculated the angle θ by ensemble-average (symbol $\langle \rangle$) for the two interfaces. $\langle \theta \rangle$ is calculated by detecting the asphaltene molecules pertaining to both interfaces and then calculating the simple average between all θ angles of each molecule at both interfaces; the result is averaged in time. Fig. 14 shows the averaged θ angle for all concentrations. It can be seen that at low concentrations ($C < 25$ g/L), the asphaltene molecules settle nearly parallel to the interfaces ($\theta < 10^\circ$), which means that there is enough space for the molecules to arrange at the interface. As the concentration increases ($C \geq 40$ g/L), the asphaltene molecules saturate, and the entropic effects dominate at the interface, which leads to an “expulsion effect”. The asphaltene molecules that migrate from interface to bulk phase (oil) carry water molecules, due to the great affinity between the asphaltene heteroatom and water. This “expulsion effect” displaces the asphaltene molecules from the interface, which increases the angle θ , as an attempt to minimize the free energy at the interfaces.

The total number of asphaltene aggregates (N) has also been calculated. The method to identify and calculate aggregates was taken from de Oliveira et al. [73]. Two asphaltene molecules are considered

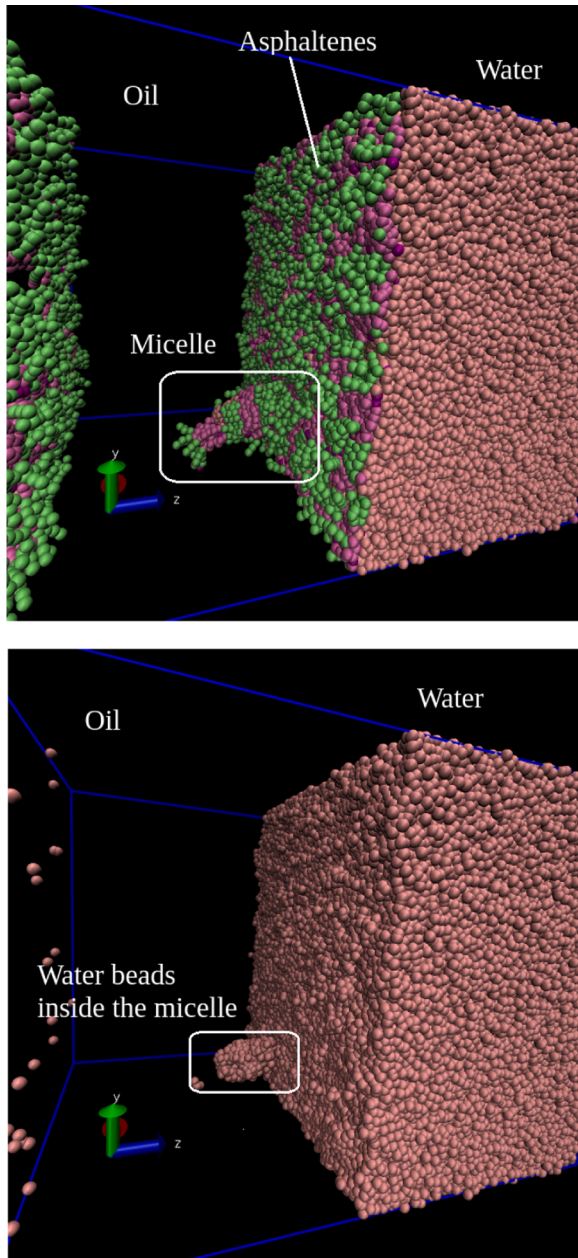


Fig. 8. Initial micelle formation of asphaltenes in water/cyclohexane interfaces. That figure shows the water in oil micelle formation with asphaltene concentration = 40 g/L. Oil (cyclohexane) beads have been omitted for better visualization.

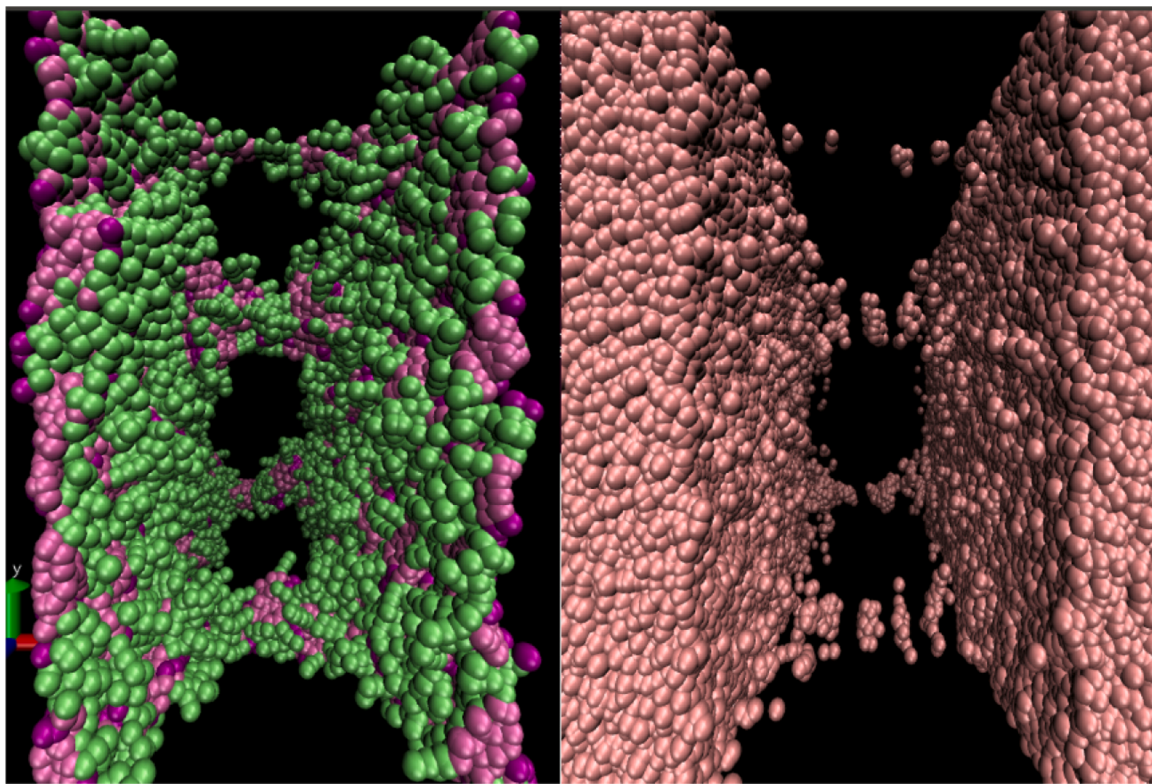


Fig. 9. Interface formed in the water/cyclohexane system with asphaltene concentration = 125.0 g/L, 298 K. The interface is supersaturated. (left) Asphaltene beads. (right) water beads. Cyclohexane (oil) beads have been omitted for better visualization.

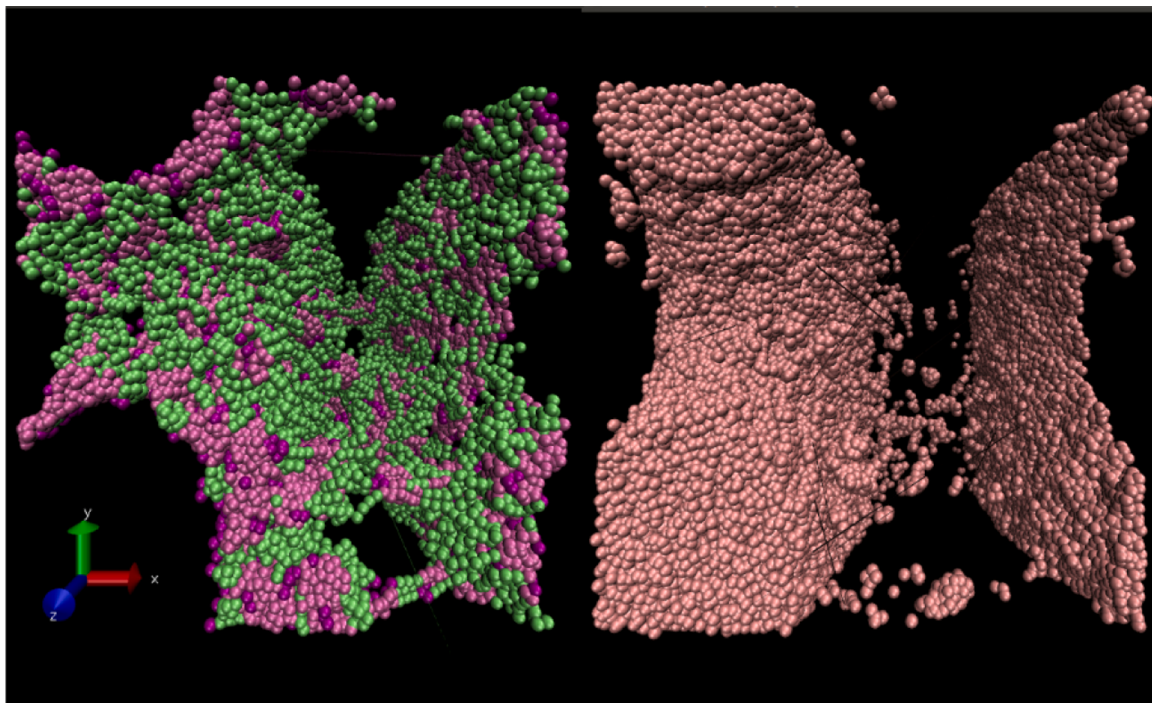


Fig. 10. Interface formed in the water/cyclohexane system with asphaltene concentration = 150.0 g/L, 298 K. The surface acquires a complex geometry that resembles droplets of a microemulsion. (left) Asphaltene beads. (right) water beads. Cyclohexane (oil) beads have been omitted for better visualization.

aggregated when the distance between the two centers of mass is less than a cutoff length. The cutoff chosen was the first minimum of $g(r)$ in Fig. 5, approximately the asphaltene aggregation distance. Fig. 15 shows N as a function of asphaltene bulk concentration. From the

graph, the number of aggregates increase with concentration, which is explained by the great number of molecules that are approaching each other. At moderate concentrations, small aggregates form large structures decreasing N . As the interface saturates, the number of

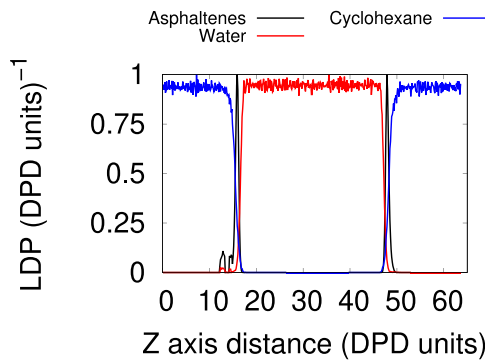


Fig. 11. Linear Density Profile (LDP) for asphaltenes at the water/cyclohexane interface. The asphaltene concentration is 40.0 g/L. The homogeneity of the two peaks means that the system is well equilibrated with the same number of molecules at each interface. The curves were normalized by their maximum values to be in the same scale. A small lateral peak in the asphaltene profile represents the water in oil micelle formation.

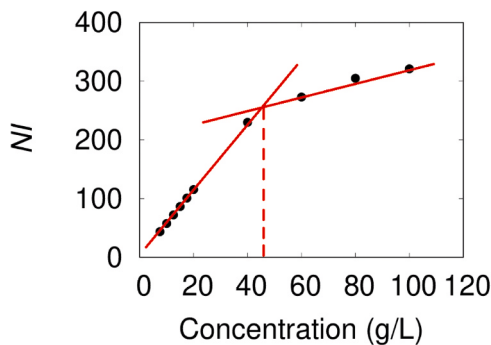


Fig. 12. Number of asphaltene molecules NI at the water/cyclohexane interface as a function of asphaltene bulk concentration. Concentrations ranging between 7.5 and 100 g/L. Higher concentrations produce higher peaks in the Linear Density Profile which increases NI , as a consequence of the great number of molecules settling at the interfaces. Red lines are to guide the eyes. (For interpretation of the references to color in this figure legend, the reader is referred to the web version of this article.)

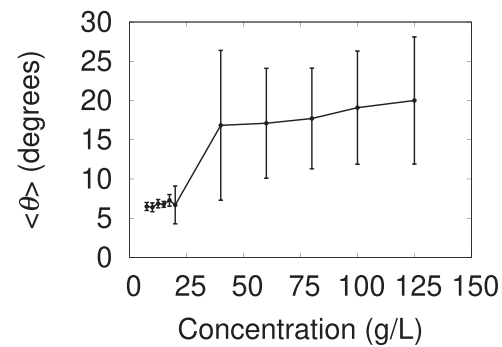


Fig. 14. $\langle \theta \rangle$ against asphaltene concentration at the water/cyclohexane interface. $\langle \theta \rangle$ is the ensemble-averaged angle between asphaltene molecular planes and the interfaces.

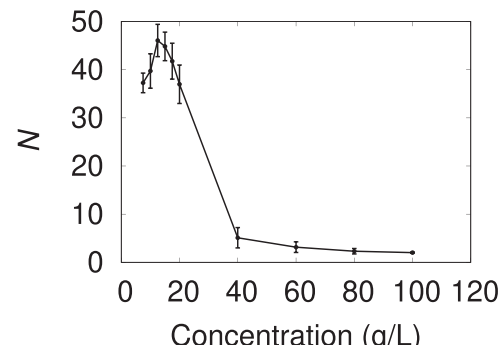


Fig. 15. Total number of asphaltene aggregates (N) as a function of asphaltene bulk concentration. Initially, the number of aggregates increase because of the great number of molecules close to each other. At higher concentrations, molecules are so close that small aggregates joint forming a few larger aggregates.

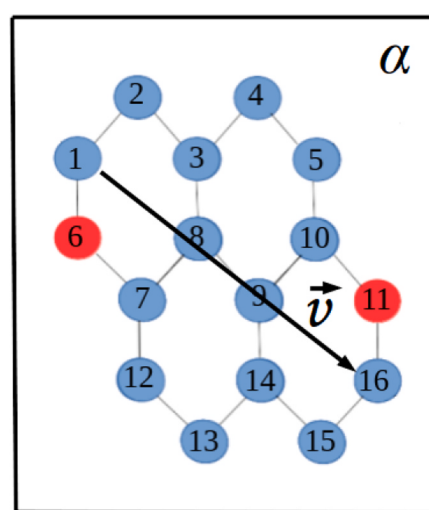


Fig. 13. Schematic representation of the separation angle θ between asphaltene molecular plane α and the interface. The molecular plane vector is defined by \vec{v} (position vector between the first (1st) and the last particle (16th) of the polyaromatic nuclei), the vector normal to the interface is \vec{n} .

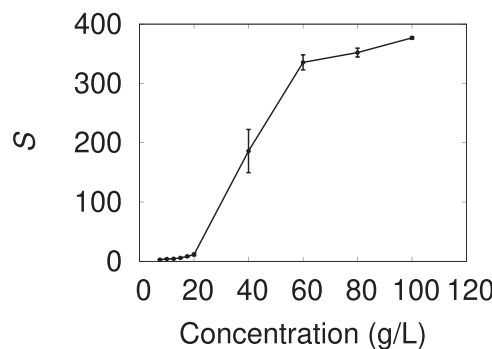


Fig. 16. Average aggregate size (S) of asphaltenes in water/cyclohexane as a function of asphaltene bulk concentration. Isolated asphaltenes aggregate until 20 g/L which increases S . From 20 g/L to 60 g/L small aggregates joint forming larger structures which greatly increases S . Concentrations above 60 g/L causes a small increase in S because the interface is saturated.

aggregates diminishes a little because molecules are too close to each other, forming only a few aggregates. Therefore at high concentrations, the graph is reaching a plateau. The average aggregate size (S) was calculated using the same algorithm. It represents the average number of asphaltene molecules in each aggregate. Fig. 16 shows the plot of S as a function of asphaltene bulk concentration. Three regions can be identified. Until 20 g/L isolated asphaltenes form small aggregates at the interface, which increases S . Between 20 and 60 g/L, S increases significantly, resulting from the condensation of small aggregates forming large aggregates with high S values. For concentration above 60 g/L the interface is too saturated; thus the increase in S is small.

5. Conclusions

The Dissipative Particle Dynamics, DPD, was used to study the interfacial properties of asphaltenes adsorbed on the water/oil interface. Cyclohexane was used as the oil phase. For unlike beads, the DPD parameters were calculated using COSMO-SAC, which has the advantage of being an open-source, generic way of estimating DPD parameters consistent with real systems. We used interface tension of several hydrocarbon-water systems to validate the methodology, showing very good agreement over a range of temperatures. To know whether the method can access the structural and the diffusion coefficient of asphaltenes in toluene, we calculated these properties and compared them with experimental data. The Radial Distribution Function and the Diffusivity obtained here agreed with the experimental data.

The Linear Density Profiles were calculated for different concentrations, showing that the interfaces are homogeneous at low asphaltene concentrations. The angle θ between asphaltene molecular planes and the interface has also been analyzed. At low asphaltene concentrations ($C < 25$ g/L), asphaltene tends to settle parallel to the interface as there are few molecules on the interface. At higher concentrations ($C \geq 40$ g/L), the asphaltene molecules are displaced over the interface due to entropic effects, which increases the angle between molecular planes and the interface. Microemulsion tends to be stable at these high asphaltene concentrations, and the interfaces start to be not well defined. The number of asphaltene aggregates N and the average size S have also been computed as a function of the asphaltene bulk concentration. The results show that initially isolated asphaltenes aggregate, which increases N and S . At intermediate concentrations, the small aggregates form large structures, increasing the S values and decreasing the number of aggregates. At high concentrations, N and S vary a little because of the interface saturation.

CRediT authorship contribution statement

Fellipe Carvalho: Original draft, Calculations, Molecular simulation, Writing - several versions. **João Maia:** Conceptualization, Supervision, DPD Software, Writing - review & editing. **Frederico W. Tavares:** Supervision, Conceptualization, Methodology, Writing - review & editing.

Declaration of Competing Interest

The authors declare that they have no known competing financial interests or personal relationships that could have appeared to influence the work reported in this paper.

Acknowledgements

This study was financed in part by the Coordenação de Aperfeiçoamento de Pessoal de Nível Superior (CAPES) - Finance Code 001. The authors Fellipe Carvalho de Oliveira and Frederico Wanderley Tavares thank to the Conselho Nacional de Desenvolvimento Científico e Tecnológico - CNPq and ANP-Petrobrás for the financial support. We thank the reviewers for the suggestions and contributions. We thank Professor Rafael de Pelegrini Soares (Federal University of Rio Grande do Sul - UFRGS) and Renan Pereira Gerber for help and the free availability of the software at <https://code.google.com/archive/p/jcosmo/>.

References

- [1] J. Jfestin, S. Simon, L. Zupancic, L. Barré, A small angle neutron scattering study of the adsorbed asphaltene layer in water-in-hydrocarbon emulsions: structural description related to stability, *Langmuir* 23 (2007) 10471–10478.
- [2] H. Sabbah, A.L. Morrow, A.E. Pomerantz, R.N. Zare, Evidence for island structures as the dominant architecture of asphaltenes, *Energy Fuels* 25 (2011) 1597–1604.
- [3] V.G. Morgan, T.M. Bastos, C.M. Sad, J.S. Leite, E.R. Castro, L.L. Barbosa, Application of low-field nuclear magnetic resonance to assess the onset of asphaltene precipitation in petroleum, *Fuel* 265 (2020), 116955, <https://doi.org/10.1016/j.fuel.2019.116955>. (<http://www.sciencedirect.com/science/article/pii/S0016236119323488>).
- [4] M. Sedighi, L. Goual, W. Welch, J. Kubelka, Effect of asphaltene structure on association and aggregation using molecular dynamics, *J. Phys. Chem. B* 117 (2013) 5765–5776.
- [5] T. Kuznicki, J.H. Masliyah, S. Bhattacharjee, Molecular dynamics study of model molecules resembling asphaltene-like structures in aqueous organic solvent systems, *Energy Fuels* 22 (2008) 2379–2389.
- [6] O.C. Mullins, The modified yen model, *Energy Fuels* 24 (2010) 2179–2207.
- [7] T. Headen, E. Boek, G. Jackson, T. Totton, E. Müller, Simulation of asphaltene aggregation through molecular dynamics: insights and limitations, *Energy Fuels* 31 (2017) 1108–1125.
- [8] S.-F. Zhang, L.-L. Sun, J.-B. Xu, H. Wu, H. Wen, Aggregate structure in heavy crude oil: using a dissipative particle dynamics based mesoscale platform, *Energy Fuels* 24 (2010) 4312–4326.
- [9] H.W. Yarranton, H. Hussein, J.H. Masliyah, Water-in-hydrocarbon emulsions stabilized by asphaltenes at low concentrations, *J. Colloid Interface Sci.* 228 (2000) 52–63.
- [10] P. Bouriat, N. El Kerri, A. Graciaa, J. Lachaise, Properties of a two-dimensional asphaltene network at the water- cyclohexane interface deduced from dynamic tensiometry, *Langmuir* 20 (2004) 7459–7464.
- [11] C.-C. Chang, A. Nowbar, V. Mansard, I. Williams, J. Mecca, A.K. Schmitt, T.H. Kalantar, T.-C. Kuo, T.M. Squires, Interfacial rheology and heterogeneity of aging asphaltene layers at the water-oil interface, *Langmuir* 34 (2018) 5409–5415. [10.1021/acs.langmuir.8b00176](https://doi.org/10.1021/acs.langmuir.8b00176). PMID: 29685033.
- [12] C. Shi, L. Zhang, L. Xie, X. Lu, Q. Liu, J. He, C.A. Mantilla, F.G. A. Van den berg, H. Zeng, Surface interaction of water-in-oil emulsion droplets with interfacially active asphaltenes, *Langmuir* 33 (2017) 1265–1274. [10.1021/acs.langmuir.6b04265](https://doi.org/10.1021/acs.langmuir.6b04265). PMID: 28081605.
- [13] J. Liu, Y. Zhao, S. Ren, Molecular dynamics simulation of self-aggregation of asphaltenes at an oil/water interface: formation and destruction of the asphaltene protective film, *Energy Fuels* 29 (2015) 1233–1242.
- [14] H. Shinto, Computer simulation of wetting, capillary forces, and particle-stabilized emulsions: from molecular-scale to mesoscale modeling, *Adv. Powder Technol.* 23 (2012) 538–547, <https://doi.org/10.1016/j.apt.2012.06.003>. (<http://www.sciencedirect.com/science/article/pii/S0921883112000763>).
- [15] S.C. Glotzer, W. Paul, Molecular and mesoscale simulation methods for polymer materials, *Annu. Rev. Mater. Res.* 32 (2002) 401–436, <https://doi.org/10.1146/annurev.matsci.32.010802.112213>.
- [16] R.D. Groot, P.B. Warren, Dissipative particle dynamics: bridging the gap between atomistic and mesoscopic simulation, *J. Chem. Phys.* 107 (1997) 4423–4435.

- [17] S.J. Marrink, H.J. Risselada, S. Yefimov, D.P. Tieleman, A.H. De Vries, The martini force field: coarse grained model for biomolecular simulations, *J. Phys. Chem. B* 111 (2007) 7812–7824.
- [18] H. Qian, L. Chen, Z. Lu, Z. Li, C. Sun, The influence of molecule flexibility and shape on the morphology of miktoarm block copolymers in two dimensions, *EPL (Europhys. Lett.)* 74 (2006) 466.
- [19] S. Yamamoto, Y. Maruyama, S.-A. Hyodo, Dissipative particle dynamics study of spontaneous vesicle formation of amphiphilic molecules, *J. Chem. Phys.* 116 (2002) 5842–5849.
- [20] F.L. Paiva, A.R. Secchi, V. Calado, J. Maia, S. Khani, Slip and momentum transfer mechanisms mediated by janus rods at polymer interfaces, *Soft Matter* 16 (2020) 6662–6672.
- [21] G. Andreatta, N. Bostrom, O.C. Mullins, High-q ultrasonic determination of the critical nanoaggregate concentration of asphaltenes and the critical micelle concentration of standard surfactants, *Langmuir* 21 (2005) 2728–2736. [10.1021/la048640t](https://doi.org/10.1021/la048640t). PMID: 15779941.
- [22] S. Chakraborty, C.K. Choudhury, S. Roy, Morphology and dynamics of carbon nanotube in polycarbonate carbon nanotube composite from dissipative particle dynamics simulation, *Macromolecules* 46 (2013) 3631–3638.
- [23] H. Rezaei, S. Amjad-Iranagh, H. Modarresi, Self-accumulation of uncharged polyaromatic surfactants at crude oil–water interface: a mesoscopic dpd study, *Energy Fuels* 30 (2016) 6626–6639.
- [24] Y. Ruiz-Morales, O.C. Mullins, Coarse-grained molecular simulations to investigate asphaltenes at the oil–water interface, *Energy Fuels* 29 (2015) 1597–1609.
- [25] C. d. V. Silva, A mesoscopic model for an asphaltene and complex mixtures of asphaltenes, *Pet. Sci. Technol.* 33 (2015) 839–845.
- [26] S. Wang, J. Xu, H. Wen, Dissipative particle dynamics simulation on the rheological properties of heavy crude oil, *Mol. Phys.* 113 (2015) 3325–3335.
- [27] J. Chen, J. Chen, C. Zhong, S. Chen, B. Chen, S. Fang, W. Xiang, Mesoscopic probes in asphaltenes nanoaggregate structure: from perpendicular to parallel orientation at the water-in-oil emulsions interface, *RSC Adv.* 7 (2017) 38193–38203.
- [28] F.C. de Oliveira, S. Khani, J.M. Maia, F.W. Tavares, Concentration and solvent effects on structural, dynamical, and rheological properties of asphaltene suspensions, *Energy Fuels* 34 (2020) 1071–1081, <https://doi.org/10.1021/acs.energyfuels.9b03315>.
- [29] R. Fingerhut, W.-L. Chen, A. Schedemann, W. Cordes, J. Rarey, C.-M. Hsieh, J. Vrabec, S.-T. Lin, Comprehensive assessment of cosmo-sac models for predictions of fluid-phase equilibria, *Ind. Eng. Chem. Res.* 56 (2017) 9868–9884, <https://doi.org/10.1021/acs.iecr.7b01360>.
- [30] C.-M. Hsieh, S.I. Sandler, S.-T. Lin, Improvements of cosmo-sac for vapor-liquid and liquid-liquid equilibrium predictions, *Fluid Phase Equilibria* 297 (2010) 90–97, <https://doi.org/10.1016/j.fluid.2010.06.011>. (<http://www.sciencedirect.com/science/article/pii/S0378381210003201>).
- [31] C.-M. Hsieh, S.-T. Lin, J. Vrabec, Considering the dispersive interactions in the cosmo-sac model for more accurate predictions of fluid phase behavior, *Fluid Phase Equilibria* 367 (2014) 109–116, <https://doi.org/10.1016/j.fluid.2014.01.032>. (<http://www.sciencedirect.com/science/article/pii/S0378381214000570>).
- [32] S.-T. Lin, S.I. Sandler, *A priori* phase equilibrium prediction from a segment contribution solvation model, *Ind. Eng. Chem. Res.* 41 (2002) 899–913.
- [33] T. Merker, C.-M. Hsieh, S.-T. Lin, H. Hasse, J. Vrabec, Fluid-phase coexistence for the oxidation of co₂ expanded cyclohexane: experiment, molecular simulation, and cosmo-sac, *AIChE J.* 59 (2013) 2236–2250, <https://doi.org/10.1002/aic.13986>. (<https://aiche.onlinelibrary.wiley.com/doi/abs/10.1002/aic.13986>).
- [34] B.-S. Lee, S.-T. Lin, Screening of ionic liquids for co₂ capture using the cosmo-sac model, *Chem. Eng. Sci.* 121 (2015) 157–168. (<http://www.sciencedirect.com/science/article/pii/S0009250914004357>). [10.1016/j.ces.2014.08.017](https://doi.org/10.1016/j.ces.2014.08.017). 2013 Danckwerts Special Issue on Molecular Modelling in Chemical Engineering.
- [35] R. d. P. Soares, The combinatorial term for cosmo-based activity coefficient models, *Ind. Eng. Chem. Res.* 50 (2011) 3060–3063, <https://doi.org/10.1021/ie102087p>.
- [36] R.P. Gerber, R. d. P. Soares, Assessing the reliability of predictive activity coefficient models for molecules consisting of several functional groups, *Braz. J. Chem. Eng.* 30 (2013) 1–11.
- [37] A. Jakob, H. Grensemann, J. Lohmann, J. Gmehling, Further development of modified unifac (dortmund): revision and extension 5, *Ind. Eng. Chem. Res.* 45 (2006) 7924–7933, <https://doi.org/10.1021/ie060355c>.
- [38] J. Gmehling, Phasengleichgewichtsmodelle zur synthese und auslegung von trennprozessen, *Chem. Ing. Tech.* 66 (1994) 792–808, <https://doi.org/10.1002/cite.330660604>. (<https://onlinelibrary.wiley.com/doi/abs/10.1002/cite.330660604>).
- [39] D. Constantinescu, J. Gmehling, Further development of modified unifac (dortmund): revision and extension 6, *J. Chem. Eng. Data* 61 (2016) 2738–2748, <https://doi.org/10.1021/acs.jced.6b00136>.
- [40] H. Alasiri, W.G. Chapman, Dissipative particle dynamics (dpd) study of the interfacial tension for alkane/water systems by using cosmo-rs to calculate interaction parameters, *J. Mol. Liq.* 246 (2017) 131–139.
- [41] H.S. Alasiri, A.S. Sultan, W.G. Chapman, Effect of surfactant headgroup, salts, and temperature on interfacial properties: dissipative particle dynamics and experiment for the water/octane/surfactant system, *Energy Fuels* 33 (2019) 6678–6688.
- [42] P. Hoogerbrugge, J. Koelman, Simulating microscopic hydrodynamic phenomena with dissipative particle dynamics, *EPL (Europhys. Lett.)* 19 (1992) 155.
- [43] D. Frenkel, B. Smit, *Understanding Molecular Simulation: From Algorithms to Applications*, vol. 1, Elsevier, 2001.
- [44] U. Frisch, B. Hasslacher, Y. Pomeau, Lattice-gas automata for the navier-stokes equation, *Phys. Rev. Lett.* 56 (1986) 1505.
- [45] P. Espanol, P. Warren, Statistical mechanics of dissipative particle dynamics, *EPL (Europhys. Lett.)* 30 (1995) 191.
- [46] R. Kubo, The fluctuation-dissipation theorem, *Rep. Prog. Phys.* 29 (1966) 255.
- [47] S. Nosé, A molecular dynamics method for simulations in the canonical ensemble, *Mol. Phys.* 52 (1984) 255–268.
- [48] S. Plimpton, Fast parallel algorithms for short-range molecular dynamics, *J. Comput. Phys.* 117 (1995) 1–19.
- [49] R.D. Groot, K. Rabone, Mesoscopic simulation of cell membrane damage, morphology change and rupture by nonionic surfactants, *Biophys. J.* 81 (2001) 725–736.
- [50] E. Mullins, R. Oldland, Y.A. Liu, S. Wang, S.I. Sandler, C.-C. Chen, M. Zwolak, K. C. Seavey, Sigma-profile database for using cosmo-based thermodynamic methods, *Ind. Eng. Chem. Res.* 45 (2006) 4389–4415. (<https://doi.org/10.1021/ie060370h>).
- [51] X. Song, P. Shi, S. Zhao, M. Duan, C. Wang, Y. Ma, Dissipative particle dynamics study on the aggregation behavior of asphaltenes under shear fields, *Ind. Eng. Chem. Res.* 55 (2016) 9077–9086.
- [52] J. Xu, S. Zhang, H. Wu, Y. Zhao, H. Wen, Mesoscopic simulation of aggregate structure and stability of heavy crude oil by gpu accelerated dpd, *Chem. Eng. Trans.* 24 (2011) 1531–1536. (<https://doi.org/10.3303/CET1124256>). (<https://www.cetjournal.it/index.php/cet/article/view/CET1124256>).
- [53] S. Wang, J. Xu, H. Wen, The aggregation and diffusion of asphaltenes studied by gpu-accelerated dissipative particle dynamics, *Comput. Phys. Commun.* 185 (2014) 3069–3078.
- [54] J. Pacheco-Sánchez, I. Zaragoza, J. Martínez-Magadán, Asphaltene aggregation under vacuum at different temperatures by molecular dynamics, *Energy Fuels* 17 (2003) 1346–1355.
- [55] P. Espanol, P.B. Warren, Perspective: dissipative particle dynamics, *J. Chem. Phys.* 146 (2017), 150901.
- [56] S. Ok, M. Mahmoodinia, N. Rajasekaran, M.A. Sabti, A. Lervik, T.S. van Erp, R. Cabriolu, Molecular structure and solubility determination of asphaltenes, *Energy Fuels* 33 (2019) 8259–8270, <https://doi.org/10.1021/acs.energyfuels.9b01737>.
- [57] A. Maiti, S. McGrother, Bead-bead interaction parameters in dissipative particle dynamics: relation to bead-size, solubility parameter, and surface tension, *J. Chem. Phys.* 120 (2004) 1594–1601.
- [58] S. Corporation, Improper Style Command, 2021. (https://lammps.sandia.gov/doc/improper_style.html/). (Accessed 2021-04-30).
- [59] A. Klamt, G. Schüürmann, Cosmo: a new approach to dielectric screening in solvents with explicit expressions for the screening energy and its gradient, *J. Chem. Soc. Perkin Trans. 2* (1993) 799–805.
- [60] A. Klamt, Conductor-like screening model for real solvents: a new approach to the quantitative calculation of solvation phenomena, *J. Phys. Chem.* 99 (1995) 2224–2235.
- [61] A. Klamt, V. Jonas, T. Bürger, J.C. Lohrenz, Refinement and parametrization of cosmo-rs, *J. Phys. Chem. A* 102 (1998) 5074–5085.
- [62] A. Klamt, F. Eckert, Cosmo-rs: a novel and efficient method for the a priori prediction of thermophysical data of liquids, *Fluid Phase Equilibria* 172 (2000) 43–72.
- [63] A. Khedr, A. Striolo, Dpd parameters estimation for simultaneously simulating water-oil interfaces and aqueous nonionic surfactants, *J. Chem. Theory Comput.* 14 (2018) 6460–6471. [10.1021/acs.jctc.8b00476](https://doi.org/10.1021/acs.jctc.8b00476). PMID: 30376315.
- [64] S. Zeppieri, J. Rodríguez, A. López de Ramos, Interfacial tension of alkane+ water systems, *J. Chem. Eng. Data* 46 (2001) 1086–1088.
- [65] E. Mayoral, A.G. Goicochea, Modeling the temperature dependent interfacial tension between organic solvents and water using dissipative particle dynamics, *J. Chem. Phys.* 138 (2013), 094703.
- [66] M. Duan, X. Song, S. Zhao, S. Fang, F. Wang, C. Zhong, Z. Luo, Layer-by-layer assembled film of asphaltenes/polyacrylamide and its stability of water-in-oil emulsions: a combined experimental and simulation study, *J. Phys. Chem. C* 121 (2017) 4332–4342.
- [67] F. Alvarez-Ramirez, E. Ramirez-Jaramillo, Y. Ruiz-Morales, Calculation of the interaction potential curve between asphaltene- asphaltene, asphaltene- resin, and resin- resin systems using density functional theory, *Energy Fuels* 20 (2006) 195–204.
- [68] A.B. Andrews, R.E. Guerra, O.C. Mullins, P.N. Sen, Diffusivity of asphaltene molecules by fluorescence correlation spectroscopy, *J. Phys. Chem. A* 110 (2006) 8093–8097.
- [69] J.-A. Östlund, M. Nydén, I.H. Auflem, J. Sjöblom, Interactions between asphaltenes and naphthenic acids, *Energy Fuels* 17 (2003) 113–119.
- [70] W. Loh, R.S. Mohamed, A.C. Ramos, Aggregation of asphaltenes obtained from a brazilian crude oil in aromatic solvents, *Pet. Sci. Technol.* 17 (1999) 147–163.
- [71] E. Rogel, O. Leon, G. Torres, J. Espidel, Aggregation of asphaltenes in organic solvents using surface tension measurements, *Fuel* 79 (2000) 1389–1394.
- [72] T. Giorgino, Computing 1-d atomic densities in macromolecular simulations: the density profile tool for vmd, *Comput. Phys. Commun.* 185 (2014) 317–322.
- [73] F.C. de Oliveira, S. Khani, J.M. Maia, F.W. Tavares, Modified clustering algorithm for molecular simulation, *Mol. Simul.* 46 (2020) 1453–1466.